CuO, MgO, and ZrO_2 Loading on HZSM5 by Deposition-precipitation: Study of Crystallinity, Specific Surface Area, and Morphology

Rizky Ibnufaatih Arvianto[1], Anatta Wahyu Budiman[1*], and Khoirina Dwi Nugrahaningtyas[2]

[1]*Department of Chemical Engineering, Faculty of Engineering, Universitas Sebelas Maret, Jl. Ir. Sutami 36A, Kentingan, Surakarta 57126, Indonesia*

[2]*Department of Chemistry, Faculty of Natural Sciences and Mathematics, Universitas Sebelas Maret, Jl. Ir. Sutami 36A, Kentingan, Surakarta 57126, Indonesia*

* ***Corresponding author:***

email: budiman@staff.uns.ac.id

Received: January 14, 2022
Accepted: March 23, 2022

DOI: 10.22146/ijc.72255

Abstract: *Bifunctional catalysts are often used in multiple reactions to synthesize certain products. The catalytic activity of bifunctional catalysts is influenced by parameters such as crystallinity, specific surface area, metal distribution, and morphology. Bifunctional catalysts are manufactured by adding metal to the support. The metal loading to the support often affects these parameters. Therefore, this research was conducted to determine the effect of CuO, MgO, and ZrO_2 addition to HZSM5 on these parameters. The often-used loading method was deposition precipitation. The pH of the metal-support precursors' solution was increased to basic (pH of 8) to deposit the metal on the support. The loading effect was investigated by producing the following materials: CuO/HZSM5, CuO/ZrO_2/HZSM5, CuO/MgO/HZSM5, and CuO/MgO/ZrO_2/HZSM5. Each material was characterized using XRD, SAA, SEM, Mapping, EDS, and XRF. The results showed that all metal oxides could be embedded in the HZSM5. The loading of CuO, MgO, and ZrO_2 to HZSM5 did not affect the crystallinity (structure) and morphology, increased the specific surface area, and was evenly distributed inside the pore of HZSM5. Further research is needed to determine the effect of crystallinity, specific surface area, and morphology on other metals and support types.*

Keywords: *crystallinity; specific surface area; morphology; deposition-precipitation*

■ INTRODUCTION

The application of catalysts in the industry is essential. Most of the chemical industry uses catalysts for certain product formations. Sustainable production requires suitable chemical processes and catalysts [1]. One of the uses of catalysts is in the DME manufacturing industry. Several industries use two reactors with the help of two catalysts, namely metal (for the CO/CO_2 hydrogenation reaction to methanol) and solid acid (for the methanol dehydration reaction to DME). However, this method requires a lot of costs [2]. Therefore, many studies have combined metals and solid acids to produce bifunctional catalysts so that reactions in two reactors can occur instantly in one reactor assisted by this catalyst. However, the metal addition to the support (solid acid) often affects the catalyst's crystallinity, specific surface area, and morphology. Meanwhile, several studies showed an excellent catalyst gives a good performance related to the high crystallinity [3], high surface area [4], porous morphology [5,6], and metal distribution on support [5,7]. Therefore, it is crucial to study the effects of metal addition to support the bifunctional catalyst of direct DME synthesis.

CuO, MgO, and ZrO_2 have impressive abilities as metal catalysts to synthesize methanol. CuO is a catalyst for methanol synthesis from CO_2 [8-9] or CO [10]. Adding MgO or ZrO_2 can increase the formation of methanol [11-12]. One of the solid acids often used in the dehydration reaction of methanol to DME is HZSM5. The selection of HZSM5 is based on a high acidic site on the surface [13-14], high stability [11], large surface area, and pore diameter (5 to 7 Å) [15].

Deposition-precipitation involves a metal precursor precipitation onto a suspended support material by increasing the pH of the metal salt solution [16]. The addition of NH_4OH (as precipitant) at room temperature is one method to increase pH steadily [4]. The metal nucleation process is induced under primary conditions, so compounds with low solubility are formed [17].

Several studies on metal addition on the support have been published. CuO, ZnO, and MgO were loaded on γ-Al_2O_3 via the deposition-precipitation method at a pH of 7. The increase in specific surface area from 79 m^2/g to 95.9 m^2/g occurred with 20% Mg. Magnesium reduced Cu agglomeration so that the metal surface area was increased. However, the loading of 20% Mg decreased the crystallinity of the catalyst by 30%. The catalyst morphology showed degradation and distortion [12]. The MgO loading into the Cu-mordenite via deposition-precipitation method at pH of 8 showed a decrease in the specific surface area proportional to the Mg loading percentage from 0.1 to 0.4% [4]. The Mg loading did not affect the crystallinity of the catalyst because Mg was maximally dispersed. Analysis using FESEM showed that the catalyst morphology was not significantly affected by the loading of MgO [4]. The CuO, ZnO, ZrO_2, and Al_2O_3 loading to γ-Al_2O_3 by the deposition-precipitation method at a pH of 7 was carried out by Ren et al. [11]. The ZrO_2 loading to the support caused a decrease in the specific surface area, from 128 m^2/g to 109 m^2/g. In addition, the ZrO_2 loading increased the Cu dispersion from 16.3% to 18.9% [11].

In this research, CuO, MgO, and ZrO_2 were loaded on HZSM5 for bifunctional catalysts manufacture, namely CuO/HZSM5, CuO/ZrO_2/HZSM5, CuO/MgO/HZSM5, and CuO/MgO/ZrO_2/HZSM5. Each material was compared to determine the effect of adding CuO, MgO, and ZrO_2. The impact of loading on crystallinity, specific surface area, and morphology was studied to obtain the high performance of bifunctional catalyst with high crystallinity, largest specific surface area, well-dispersed metals, and porous morphology.

■ EXPERIMENTAL SECTION

Materials

Zeolite type HZSM5 99% (Si/Al = 26) from ACS material was used as catalyst support. $Cu(NO_3)_2{\cdot}3H_2O$ 99%, $MgCl_2{\cdot}6H_2O$ 99%, and $ZrOCl_2{\cdot}8H_2O$ 99% from Merck were used as the CuO, MgO, and ZrO_2 precursors.

Instrumentation

Materials were characterized by X-ray Diffractometer (XRD) Rigaku Miniflex 600 to investigate the effect of metal oxides loading on the crystallinity and X-ray Fluorescence (XRF) BRUKER S2 Ranger to determine the metal oxide content (wt.%). Crystallinity was determined using the XRD spectra of each material. Calculation of crystallinity was performed using Eq. (1):

$$\%\ \text{Crystallinity} = \frac{\text{area of crystalline peaks}}{\text{Total area (crystalline and amorphous)}} \quad (1)$$

XRD analysis was conducted at a Bragg angle of 5–90° (2θ) at room temperature. Refinement analysis was performed using Le Bail Methods with Rietica software to find the best fitting with the ICSD standard. The similarity between XRD Data and ICSD standard was represented as Rp and Rwp.

The nitrogen adsorption-desorption technique measured the material's surface area. The instrument used was Quantachrome NovaWin Version 11.04. The multi-point BET method was used to calculate the specific surface area using Eq. (2):

$$S_{BET}\ (m^2/g) = \frac{4.355}{\text{intercept} + \text{gradient}} \quad (2)$$

The metal oxides loading effect on the morphology of materials was characterized by Scanning Electron Microscopy-Mapping-Energy Dispersive Spectroscopy (Phenom Desktop ProXL). The use of SEM images to determine porosity and particle diameter distribution. Surface porosity analysis was determined by the literature using SEM data [18-20]. Porosity can be calculated by Eq. (3).

$$\text{Porosity}\ (\%) = \frac{\text{Volume of pores}}{\text{Total volume}} \times 100 \quad (3)$$

The diameter of each particle depicted in the SEM image was measured by ImageJ software and processed by OriginPro 2021 software to determine the diameter distribution of particles [20].

Procedure

The mixture of metal and HZSM5 precursors was prepared according to Table 1. Firstly, each metal precursor was dissolved in the distilled water and placed in a 250 mL beaker glass over a hot plate heater with stirring. After the solution was dissolved entirely, HZSM5 was added to the solution. The solution pH was adjusted to 8 by adding NH_4OH 0.05 M. The solution was stirred at 400 rpm, 85–90 °C for 2 h. A slurry solution was cooled to room temperature and filtered by a Buchner filter. An evaporator dried the wet solid at 60 °C for 6 h. Then, the dry solid was calcinated at 550 °C for 4 h.

■ RESULTS AND DISCUSSION

The impregnation of CuO, MgO, and ZrO_2 on HZSM5 was performed using the deposition-precipitation technique. The loading scheme is explained in Fig. 1. The effect of these metal oxides loading was tested for crystallinity, specific surface area, and morphology.

XRD and XRF Analysis

Fig. 2 shows the XRD spectra of the support before and after loading. The peaks at 2θ (°) 7.95, 8.79, 23.01, 23.84, 24.54, and 45.18° support XRD spectra are identical to HZSM5 [21-23]. After metal oxides loading, there was no change in these peaks because metal oxides loading did not damage the structure of HZSM5.

Table 2 shows the effect of CuO, MgO, and ZrO_2 loading on crystallinity. The crystallinity did not significantly change after metal oxides loading compared with the support (HZSM5). It proves that the metal oxides loading did not damage the structure of HZSM5.

The characteristic peaks of CuO, MgO, and ZrO_2 are not visible in the XRD spectra (Fig. 2) because they were evenly dispersed over the HZSM5 surface [23-24]. The same results were also obtained by Tursunov et al. [23], Din et al. [4], and Magomedowa et al. [24].

Refinement analysis was shown by The Le Bail plot in Fig. 3. The similarity between the experimental XRD

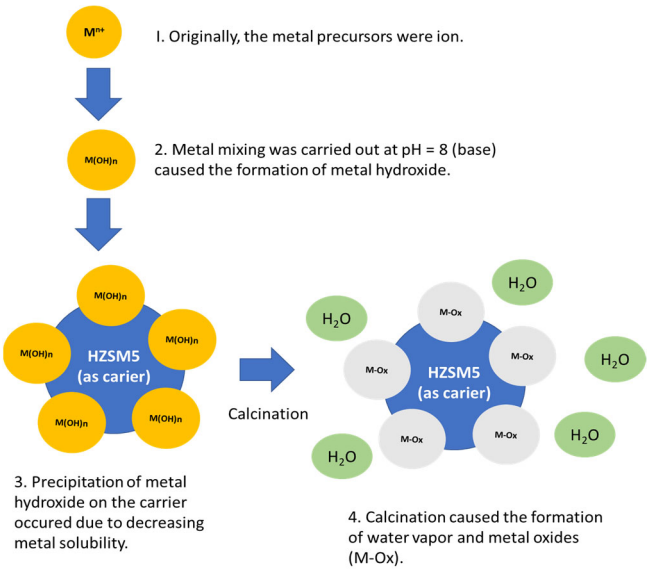

Fig 1. Scheme of CuO, MgO, and ZrO_2 formation

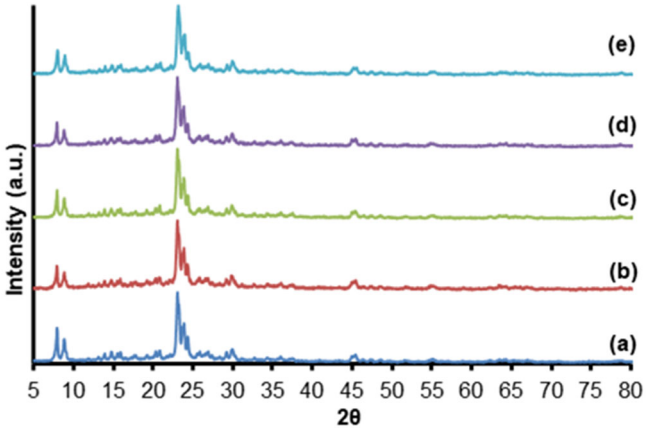

Fig 2. XRD spectra of materials: (a) HZSM5, (b) CuO/HZSM5, (c) CuO/MgO/HZSM5, (d) CuO/ZrO_2/HZSM5, (e) CuO/MgO/ZrO_2/HZSM5

Table 1. Composition of metal and HZSM5 precursors

Materials	Precursor			
	$Cu(NO_3)_2{\cdot}3H_2O$ (g)	$MgCl_2{\cdot}6H_2O$ (g)	$ZrOCl_2{\cdot}8H_2O$ (g)	HZSM5 (g)
CuO/HZSM5	1.9	-	-	10
CuO/MgO/HZSM5	1.9	0.8	-	10
CuO/ZrO_2/HZSM5	1.9	-	0.4	10
CuO/MgO/ZrO_2/HZSM5	1.9	0.8	0.4	10

Table 2. Crystallinity

Materials	Crystallinity (%)
HZSM5	79
CuO/HZSM5	79
CuO/ZrO_2/HZSM5	81
CuO/MgO/HZSM5	81
CuO/MgO/ZrO_2/HZSM5	81

pattern data and standard ICSD data were analyzed using the Le Bail method with Rietica software. The smaller value of Rp and Rwp represented that the standard tested is acceptable.

Each Le Bail plot in Fig. 3 shows a Rp and Rwp below 10. These results indicate a good fitting between the XRD spectra and the tested ICSD standard [25-26]. Refinement analysis exhibited a good fitting between HZSM5 and ICSD 61010 (space group symmetry: Pn21a, orthorhombic crystal system, lattice parameters: a = 20.09 Å; b = 19.97 Å; c = 13.36 Å, angle between axes: α = β = γ = 90° and Z = 1), CuO and ICSD 1381 (space group symmetry: I41, tetragonal crystal system, lattice parameters: a = b = 5.817 Å; c = 9.893 Å, angle between axes: α = β = γ = 90° and Z = 1), MgO and ICSD 159376 (space group symmetry: Fm-3m, cubic crystal system, lattice parameters: a = b = c = 4.212 Å, angle between axes: α = β = γ = 90° and Z = 4), ZrO_2 and ICSD 57451 (space group symmetry: C1, monoclinic crystal system, lattice parameters: a = 5.1459 Å; b = 5.2115 Å; c = 5.3128 Å, angle

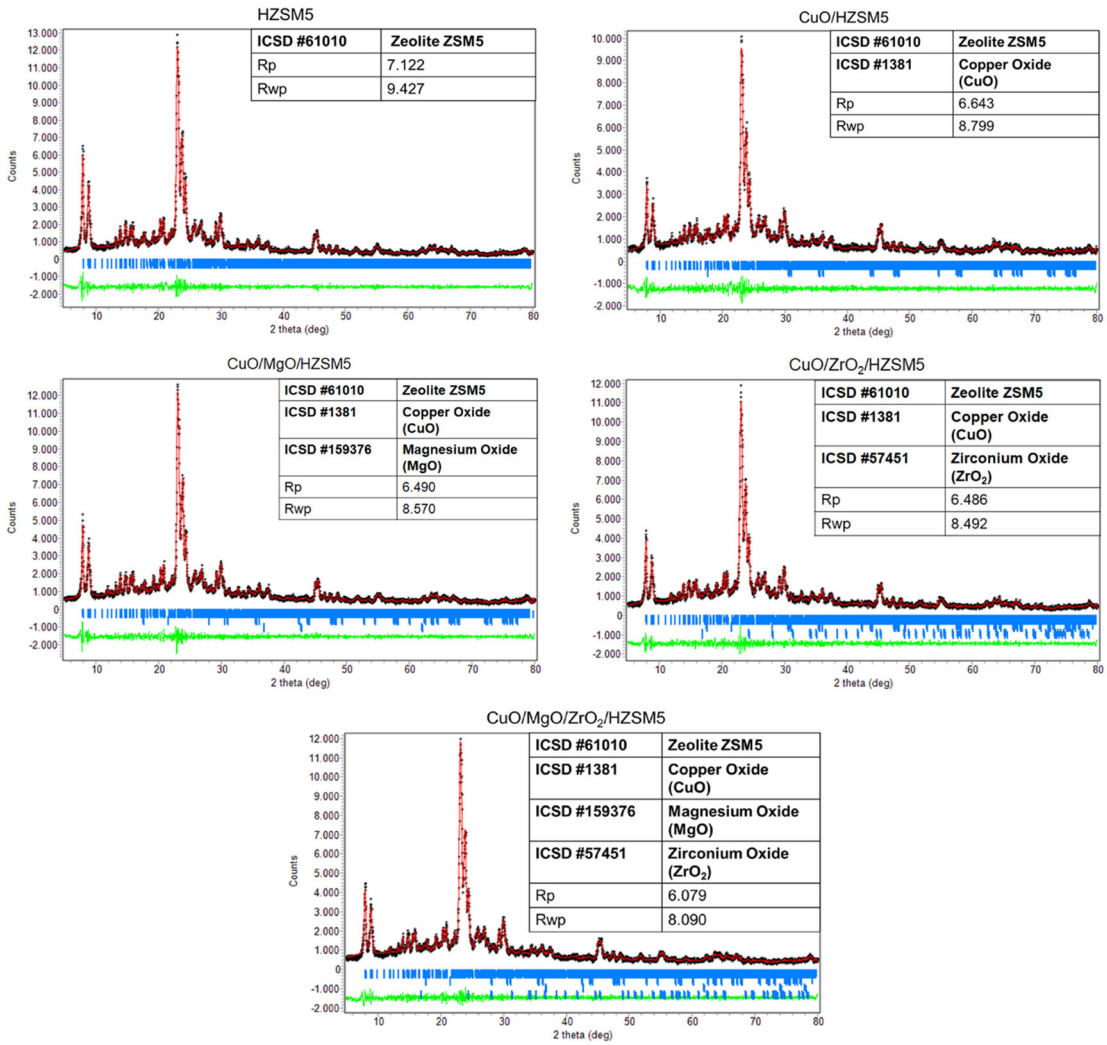

Fig 3. The Le Bails plot-supported XRD data with ICSD standard. XRD data (black); ICSD standard peaks (blue); calculation result (red); difference experiment data and calculation result (green)

Table 3. Lattice parameter and cell volume of HZSM5 before and after metal oxide addition

Materials	Lattice parameter (Å)			Cell volume (Å^3)
	a	b	c	
HZSM5	20.088	19.903	13.392	5340.515
CuO/HZSM5	20.098	19.891	13.387	5351.538
CuO/MgO/HZSM5	20.131	19.908	13.389	5365.801
CuO/ZrO_2/HZSM5	20.127	19.893	13.372	5353.833
CuO/MgO/ZrO_2/HZSM5	20.184	19.908	13.389	5370.292

between axes: α = 90°; β= 99.222°; γ = 90° and Z = 4).

The CuO, MgO, and ZrO_2 addition caused a decrease in Rp and Rwp. Adding three metal oxides at once to HZSM5 showed the most reduction in Rp and Rwp. The reduction of residual factor value (Rp and Rwp) indicates the metal oxides' existence and the stability of the support (HZSM5) [25].

The metal oxides addition in HZSM-5 caused a stretching and contraction of the lattice parameters (Table 3). It indicates the presence of metal oxide insertion in HZSM5. The lattice parameter value of support before and after metal oxide loading was not significantly different, indicating the stability of the HZSM5 structure [25]. Meanwhile, the increase in cell volume also suggests the occurrence of metal oxide embedding in HZSM5 [25].

Table 4 represents a metal oxide content in HZSM5 and CuO/MgO/ZrO_2/HZSM5. SiO_2 and Al_2O_3 contents decreased because of the total mass increase after CuO, MgO, and ZrO_2 loading. Based on XRF analysis, CuO, MgO, and ZrO_2 were successfully added to HZSM5 in 10.62, 6.40, and 6.60%, respectively.

Surface Area Analysis

Fig. 4 shows the multi-point BET graph. Based on Fig 4, it can be seen that each material has a linear graph. Table 5 represents the support-specific surface area (HZSM5) before and after metal oxides loading. The CuO, ZrO_2, and MgO loading to the support caused an increase in the specific surface area. The S_{BET} value of the support (HZSM5) is lower than other materials. The increase in the specific surface area exhibits that metal oxides did not cover the support's pores [3,27], were evenly distributed on the support [3], and did not cause damage to the support [28-29].

The loading of MgO or ZrO_2 to CuO/HZSM5 produces in different specific surface areas. The specific the surface area of CuO/MgO/HZSM5 is larger than

Table 4. XRF data of HZSM5 and CuO/MgO/ZrO_2/HZSM5

Compounds	HZSM5 (wt.%)	CuO/MgO/ZrO_2/HZSM5 (wt.%)
SiO_2	96.19%	74.4%
Al_2O_3	2.81 %	0.98%
CuO	-	10.62%
MgO	-	6.40%
ZrO_2	-	6.60%

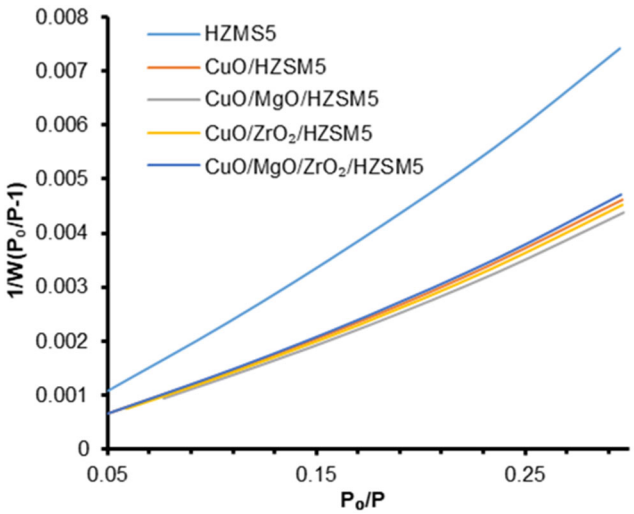

Fig 4. Multi-point BET Graph

Table 5. Surface area analysis

Material	S_{BET} (m^2/g)
HZSM5	171.457
CuO/HZSM5	275.633
CuO/ZrO_2/HZSM5	280.968
CuO/MgO/HZSM5	286.513
CuO/MgO/ZrO_2/HZSM5	270.497

$CuO/ZrO_2/HZSM5$ due to the different sizes of MgO and ZrO_2. MgO has a smaller size than ZrO_2, so MgO is more evenly distributed than ZrO_2 and does not excessively cover the pores of HZSM5. The CuO, MgO, and ZrO_2 loading at once to the HZSM5 causes a lower specific surface area than $CuO/MgO/HZSM5$ and $CuO/ZrO_2/HZSM5$ because more metal oxides were deposited on the support surface, resulting in some of them entering the pores.

Morphology Analysis

Fig. 5 shows SEM images of HZSM5 and $CuO/MgO/ZrO_2/HZSM5$. HZSM5 has a spherical morphology. The CuO, MgO, and ZrO_2 loading to HZSM5 did not affect its morphology because of the unchanged morphology of $CuO/MgO/ZrO_2/HZSM5$, as seen in Fig. 5(b) and 5(d). The same results were also obtained by the research of Din et al. and Ren et al., in which they have successfully loaded CuO, MgO, and ZrO_2 to the support without damaging or affecting the material morphology [4,11].

The $CuO/MgO/ZrO_2/HZSM5$ EDS spectra show the appearance of new peaks from Cu, Mg, and Zr compared to the HZSM5 EDS spectra (Fig. 6). These results prove the success of loading CuO, MgO, and ZrO_2 on HZSM5 (presented as total metal). The decrease in Si, Al, and O content was caused by an increase in the total mass of the material after adding Cu, Mg, and Zr. Based on EDS analysis, Cu, Mg, and Zr were deposited at 48.56, 0.14, and 0.55%, respectively.

SEM images of HZSM5 and $CuO/MgO/Zr/HZSM5$ in Fig. 5 (with 10000× magnification) were used to calculate surface porosity. Table 6 shows the surface porosity of HZSM5 and $CuO/MgO/Zr/HZSM5$, i.e., 55 and 53%, respectively. There was no significant change in the material's surface porosity after CuO, MgO, and ZrO_2 loading. Therefore, it can be concluded that the loading of CuO, MgO, and ZrO_2 to HZSM5 did not change the morphology or excessively close up the pores. The result follows the description of the surface area analysis, which shows that the metal oxides did not enter the support pores. The insignificant change in surface porosity indicates the absence of volume and pore diameter expansion. Therefore, metal oxides loading does

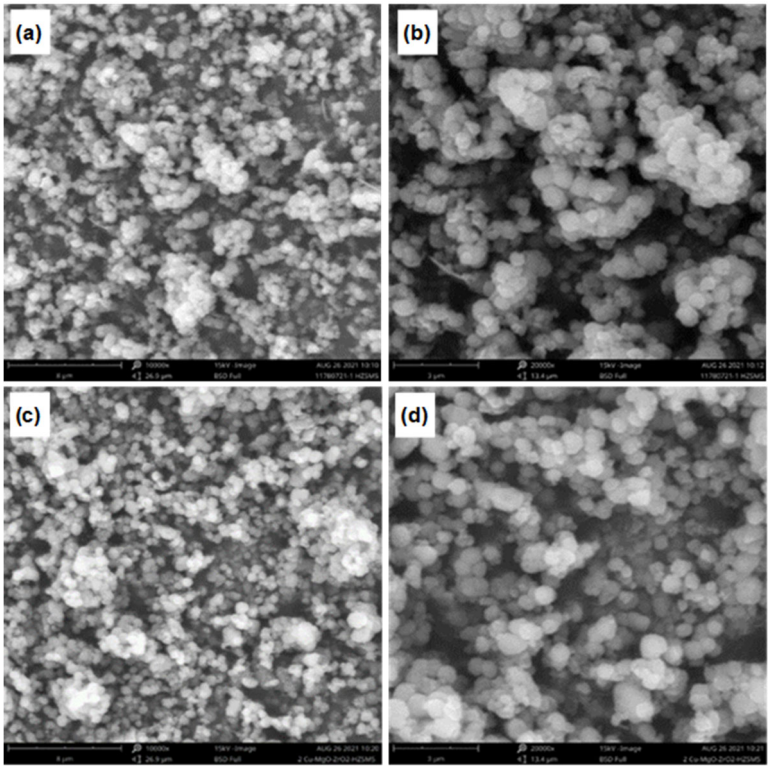

Fig 5. SEM Images of HZSM5 (a) 10000×, (b) 20000×; and $CuO/MgO/ZrO_2/HZSM5$ (c) 10000×, (d) 20000×

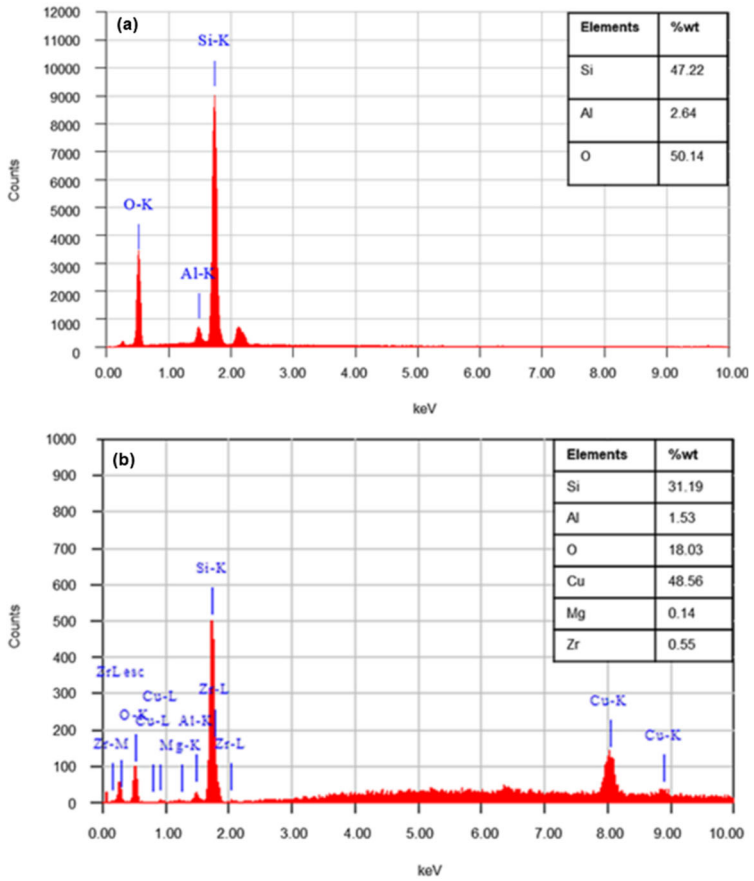

Fig 6. EDS Spectra: (a) HZSM5 and (b) CuO/MgO/ZrO_2/HZSM5

Table 6. Surface porosity analysis by SEM images

Materials	Porosity (%)
HZSM5	55
CuO/MgO/ZrO_2/HZSM5	53

not cause isomorphic substitution with Si^{4+} in the framework [30].

The measurement of particle diameter distribution was done by ImageJ software using SEM images. Fig. 7 shows the diameter distribution for HZSM5 and CuO/MgO/ ZrO_2/HZSM5. Each image has a peak that shows the highest diameter value. The peak of HZSM5 ranged from 0.5–0.55 μm. The loading of CuO, MgO, and ZrO_2 to HZSM5 caused the peak to shift to 0.7–0.8 μm. The peak shifting shows an increase in HZSM5 size due to CuO, MgO, and ZrO_2 on its surface.

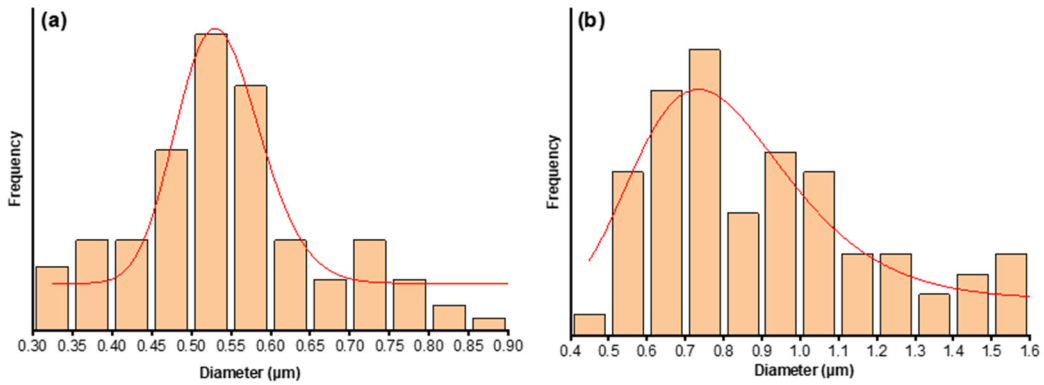

Fig 7. Diameter Distribution of (a) HZSM5 and (b) CuO/MgO/ZrO_2/HZSM5

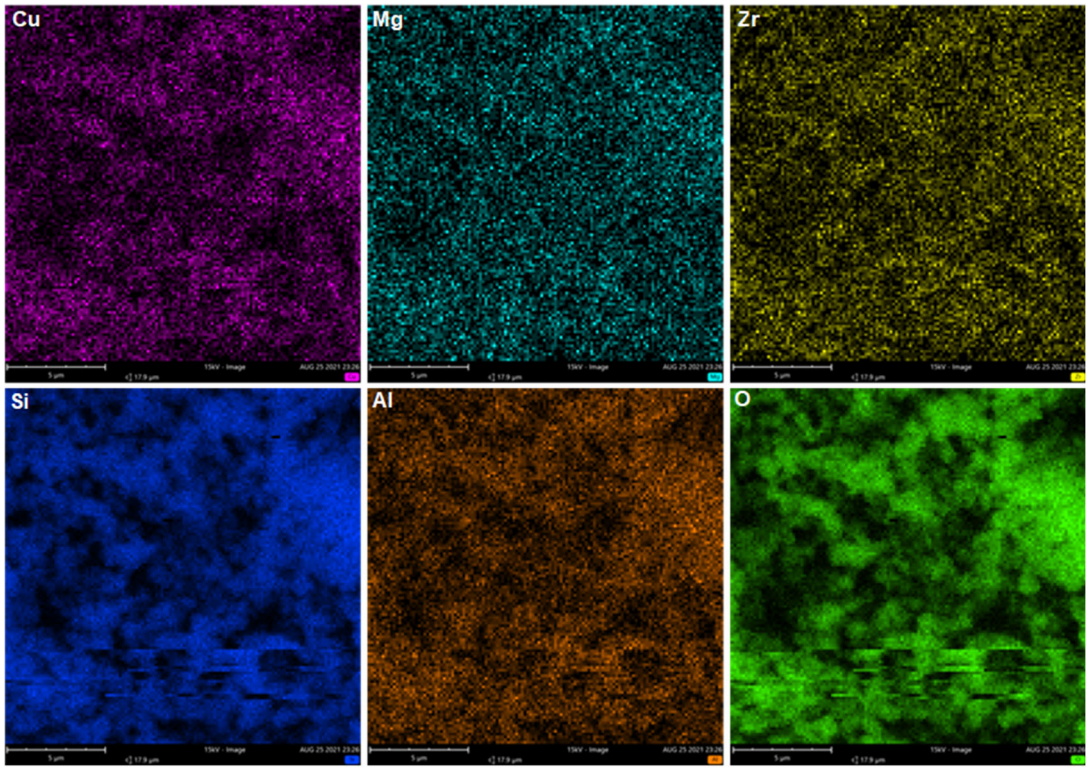

Fig 8. Elemental Mapping of CuO/MgO/ZrO_2/HZSM5

Fig. 8 shows the elemental mapping in the CuO/MgO/ZrO_2/HZSM5. According to Fig. 8, CuO, MgO, and ZrO_2 are evenly dispersed over HZSM5. In addition, these metal oxides did not form the clusters, indicating metal agglomeration on the carrier [31]. The metal oxides do not form agglomerates because they are dispersed on the support (HZSM5), thereby establishing metal oxides-support interactions and reducing metal oxides-metal oxides interactions. Therefore, the metal oxides will separate from their group (reduced agglomeration) [32].

■ CONCLUSION

CuO, MgO, and ZrO_2 have been successfully loaded to HZSM5, evidenced by the shifts of highest diameters particles, from 0.5–0.55 m to 0.7–0.8 m. XRF, XRD refinement, Mapping, and EDS analysis also exhibited the success of these metal oxides loading on the HZSM5. These metal oxides did not close the HZSM5's pores and were evenly distributed over the HZSM5 surface. Hence, the specific surface area increased, and HZSM5's porosity did not change drastically after the loading (the porous material still exists). According to the XRD data, metal oxides loading did not affect the crystallinity of HZSM5. The similarity in the XRD pattern before and after loading proved that the metal oxide addition did not damage the HZSM5 structure. XRD refinement also confirmed the stability of the HZSM5 structure by the decrease in the Rp and Rwp value after metal oxide loading. Further research can be carried out with other support and types of metal.

■ ACKNOWLEDGMENTS

This research was supported by grants from The Ministry of Education, Culture, Research and Technology of Republic Indonesia under Excellence Basic Research of Universities (PDUPT) 2021 with contract number 11/E1/KP.PTNBH/2021 and 221.1/UN27.22/HK.07.00/2021.

■ AUTHOR CONTRIBUTIONS

All authors were involved in the preparation and design of the study. Rizky Ibnufaatih Arvianto was a research assistant who conducted experiments, analyzed

data, and wrote journals. Anatta Wahyu Budiman was the head of the research team. Khoirina Dwi Nugrahaningtyas was a member of the research team. All authors contributed to the improvement of the manuscript. All authors approve the final version of the manuscript and agree to be responsible for its content.

■ REFERENCES

[1] Medford, A.J., Vojvodic, A., Hummelshøj, J.S., Voss, J., Abild-Pedersen, F., Studt, F., Bligaard, T., Nilsson, A., and Nørskov, J.K., 2015, From the Sabatier principle to a predictive theory of transition-metal heterogeneous catalysis, *J. Catal.*, 328, 36–42.

[2] Kartohardjono, S., Adji, B.S., and Muharam, Y., 2020, CO_2 utilization process simulation for enhancing production of dimethyl ether (DME), *Int. J. Chem. Eng.*, 2020, 9716417.

[3] Kristiani, A., Sudiyarmanto, S., Aulia, F., Nurul Hidayati, L., and Abimanyu, H., 2017, Metal supported on natural zeolite as catalysts for conversion of ethanol to gasoline, *MATEC Web Conf.*, 101, 01001.

[4] Din, I.U., Alotaibi, M.A., and Alharthi, A.I., 2020, Green synthesis of methanol over zeolite based Cu nano-catalysts, effect of Mg promoter, *Sustainable Chem. Pharm.*, 16, 100264.

[5] Frusteri, L., Bonura, G., Cannilla, C., Todaro, S., Giordano, G., Migliori, M., and Frusteri, F., 2020, Promoting direct CO_2 conversion to DME over zeolite-based hybrid catalysts, *Pet. Chem.*, 60 (4), 508–515.

[6] Frusteri, F., Migliori, M., Cannilla, C., Frusteri, L., Catizzone, E., Aloise, A., Giordano, G., and Bonura, G., 2017, Direct CO_2-to-DME hydrogenation reaction: New evidences of a superior behaviour of FER-based hybrid systems to obtain high DME yield, *J. CO_2 Util.*, 18, 353–361.

[7] Liu, Y., and Lu, H., 2020, Synthesis of ZSM-5 zeolite from fly ash and its adsorption of phenol, quinoline and indole in aqueous solution, *Mater. Res. Express*, 7 (5), 055506.

[8] Jiang, Q., Liu, Y., Dintzer, T., Luo, J., Parkhomenko, K., and Roger, A.C., 2020, Tuning the highly dispersed metallic Cu species via manipulating Brønsted acid sites of mesoporous aluminosilicate support for CO_2 hydrogenation reactions, *Appl. Catal., B*, 269, 118804.

[9] Chen, D., Mao, D., Wang, G., Guo, X., and Yu, J., 2019, CO_2 hydrogenation to methanol over CuO-ZnO-ZrO_2 catalyst prepared by polymeric precursor method, *J. Sol-Gel Sci. Technol.*, 89 (3), 686–699.

[10] Yanti, F.M., Valentino, N., Juwita, A.R., Murti, S.D.S., Pertiwi, A., Rahmawati, N., Rini, T.P., Sholihah, A., Prasetyo, J., Saputra, H., Iguchi, S., and Noda, R., 2020, Methanol production from biomass syngas using Cu/ZnO/Al_2O_3 catalyst, *AIP Conf. Proc.*, 2223, 020006.

[11] Ren, S., Fan, X., Shang, Z., Shoemaker, W.R., Ma, L., Wu, T., Li, S., Klinghoffer, N.B., Yu, M., and Liang, X., 2020, Enhanced catalytic performance of Zr modified CuO/ZnO/Al_2O_3 catalyst for methanol and DME synthesis via CO_2 hydrogenation, *J. CO_2 Util.*, 36, 82–95.

[12] Asthana, S., Samanta, C., Bhaumik, A., Banerjee, B., Voolapalli, R.K., and Saha, B., 2016, Direct synthesis of dimethyl ether from syngas over Cu-based catalysts: Enhanced selectivity in the presence of MgO, *J. Catal.*, 334, 89–101.

[13] Palomo, J., Rodríguez-Mirasol, J., and Cordero, T., 2019, Methanol dehydration to dimethyl ether on Zr-loaded P-containing mesoporous activated carbon catalysts, *Materials*, 12 (13), 2204.

[14] Cheng, K., Zhou, W., Kang, J., He, S., Shi, S., Zhang, Q., Pan, Y., Wen, W., and Wang, Y., 2017, Bifunctional catalysts for one-step conversion of syngas into aromatics with excellent selectivity and stability, *Chem*, 3 (2), 334–347.

[15] Widayat, W., and Annisa, A.N., 2017, Synthesis and characterization of ZSM-5 catalyst at different temperatures, *IOP Conf. Ser.: Mater. Sci. Eng.*, 214, 012032.

[16] Barton, R.R., Carrier, M., Segura, C., Fierro, J.L.G., Escalona, N., and Peretti, S.W., 2017, Ni/HZSM-5 catalyst preparation by deposition-precipitation. Part 1. Effect of nickel loading and preparation conditions on catalyst properties, *Appl. Catal., A*, 540, 7–20.

[17] Munnik, P., de Jongh, P.E., and de Jong, K.P., 2015, Recent developments in the synthesis of supported catalysts, *Chem. Rev.*, 115 (14), 6687–6718.

[18] Abdullah, M., and Khairurrijal, K., 2009, A simple method for determining surface porosity based on SEM images using OriginPro software, *Indones. J. Phys.*, 20 (2), 37–40.

[19] Hennemann, M., Gastl, M., and Becker, T., 2021, Optical method for porosity determination to prove the stamp effect in filter cakes, *J. Food Eng.*, 293, 110405.

[20] Saraf, S., Singh, A., and Desai, B.G., 2019, Estimation of porosity and pore size distribution from scanning electron microscope image data of shale samples: A case study on Jhuran formation of Kachchh Basin, India, *ASEG Extended Abstracts*, 2019 (1), 1–3.

[21] Xu, Y., Liu, J., Ma, G., Wang, J., Lin, J., Wang, H., Zhang, C., and Ding, M., 2018, Effect of iron loading on acidity and performance of Fe/HZSM-5 catalyst for direct synthesis of aromatics from syngas, *Fuel*, 228, 1–9.

[22] Lin, B., Wang, J., Huang, Q., Ali, M., and Chi, Y., 2017, Aromatic recovery from distillate oil of oily sludge through catalytic pyrolysis over Zn modified HZSM-5 zeolites, *J. Anal. Appl. Pyrolysis*, 128, 291–303.

[23] Tursunov, O., Kustov, L., and Tilyabaev, Z., 2019, Catalytic activity of H-ZSM-5 and Cu-HZSM-5 zeolites of medium SiO_2/Al_2O_3 ratio in conversion of *n*-hexane to aromatics, *J. Pet. Sci. Eng.*, 180, 773–778.

[24] Magomedova, M., Galanova, E., Davidov, I., Afokin, M., and Maximov, A., 2019, Dimethyl ether to olefins over modified ZSM-5 based catalysts stabilized by hydrothermal treatment, *Catalysts*, 9 (5), 485.

[25] Nugrahaningtyas, K.D., Putri, M.M., and Saraswati, T.E., 2020, Metal phase and electron density of transition metal/HZSM-5, *AIP Conf. Proc.*, 2237, 020003.

[26] Ozaki, Y., Suzuki, Y., Hawai, T., Saito, K., Onishi, M., and Ono, K., 2020, Automated crystal structure analysis based on blackbox optimisation, *Npj Comput. Mater.*, 6 (1), 75.

[27] Amin, M.H., Putla, S., Bee Abd Hamid, S., and Bhargava, S.K., 2015, Understanding the role of lanthanide promoters on the structure-activity of nanosized Ni/γ-Al_2O_3 catalysts in carbon dioxide reforming of methane, *Appl. Catal., A*, 492, 160–168.

[28] Rodríguez-Martínez, C., García-Domínguez, Á.E., Guerrero-Robles, F., Saavedra-Díaz, R.O., Torres-Torres, G., Felipe, C., Ojeda-López, R., Silahua-Pavón, A., and Cervantes-Uribe, A., 2020, Synthesis of supported metal nanoparticles (Au/TiO_2) by the suspension impregnation method, *J. Compos. Sci.*, 4 (3), 89.

[29] Liu, N., Chen, G., Dong, W., Liu, C., and Xu, C., 2017, Preparation of Au nanoparticles with high dispersion and thermal stability by a controlled impregnation method for alcohol oxidation, *Gold Bull.*, 50 (2), 163–175.

[30] Brazovskaya, E.Y., and Golubeva, O.Y., 2017, Study of the effect of isomorphic substitutions in the framework of zeolites with a Beta structure on their porosity and sorption characteristics, *Glass Phys. Chem.*, 43 (4), 357–362.

[31] Fakruldin, A., Ramli, A., and Abdul Mutalib, M.I., 2018, Effect of preparation method on physicochemical properties of Fe/zeolite catalyst, *J. Phys.: Conf. Ser.*, 1123, 012061.

[32] Błaszczak, P., Mizera, A., Bochentyn, B., Wang, S.F., and Jasiński, P., 2022, Preparation of methanation catalysts for high temperature SOEC by β-cyclodextrin-assisted impregnation of nano-CeO_2 with transition metal oxides, *Int. J. Hydrogen Energy*, 47 (3), 1901–1916.